Journal of Biomedical Materials Research Part A

Novel self-gelling injectable hydrogel/alpha-TCP composites for bone regeneration: physiochemical and micro-computer tomographical characterization

Journal:	*Journal of Biomedical Materials Research: Part A*
Manuscript ID	JBMR-A-17-0475.R1
Wiley - Manuscript type:	Original Article
Date Submitted by the Author:	n/a
Complete List of Authors:	Douglas, Timothy; Ghent University, Department of Molecular Biotechnology Schietse, Josefien; Ghent University, Department of Molecular Biotechnology Zima, Aneta; AGH Oniversity of Science and Technology, Faculty of Materials Science and Ceramics Gorodzha, Svetlana; National Research Tomsk Polytechnic University, Dept. Theoretical and Experimental Physics Parakhonskiy, Bogdan; Ghent University, Department of Molecular Biotechnology Khalenkow, Dmitry; Ghent University, Department of Molecular Biotechnology Shkarin, Roman; Karlsruhe Institute of Technology, Laboratory for Applications of Synchrotron Radiation, Ivanova, Anna; Rossijskaa akademia nauk, Shubnikov Institute of Crystallography Weinhardt, Venera; University of Heidelberg, Centre for Organismal Studies Baumbach, Tilo; Karlsruhe Institute of Technology, Laboratory for Applications of Synchrotron Radiation, Stevens, Christian; Universiteit Gent, Department of Sustainable Organic Chemistry and Technology Vanhoorne, Valerie; Ghent University, Department of Pharmaceutics Vervaet, Chris; Ghent University, Department of Pharmaceutics Balcaen, Lieve; Ghent University, Department of Analytical Chemistry Vanhaecke, Frank; Ghent University, Department of Analytical Chemistry Œlósarczyk, Anna; AGH-University of Science and Technology, Faculty of Materials Science and Ceramics Surmeneva, Maria; National Research Tomsk Polytechnic University, Dept. Theoretical and Experimental Physics Surmenev, Roman; National Research Tomsk Polytechnic University, Dept. Theoretical and Experimental Physics Skirtach, Andre; Ghent University, Molecular Biotechnology
Keywords:	hydrogel, composite, micro-CT, gellan gum, bone cement

Novel self-gelling injectable hydrogel/alpha-TCP composites for bone regeneration: physiochemical and micro-computer tomographical characterization

Timothy E.L. Douglas[1,2*], Josefien Schietse[1], Aneta Zima[3], Svetlana Gorodzha[4], Bogdan V. Parakhonskiy[1,5,6], Dmitry Khalenow[1], Roman Shkarin[7], Anna Ivanova[5], Tilo Baumbach[7,8], Venera Weinhardt[7,8,9], Christian V. Stevens[10], Valérie Vanhoorne[11], Chris Vervaet[11], Lieve Balcaen[12], Frank Vanhaecke[12], Anna Słośarczyk[2], Maria A. Surmeneva[4], Roman A. Surmenev[4], Andre G. Skirtach[1,13]

[1]Dept. Molecular Biotechology, Ghent University, Belgium, [2]Engineering Dept., Lancaster University, UK, [3]Dept. Ceramics and Refractories, AGH University of Science and Technology, Kraków, Poland, [4]Dept. of Experimental Physics, National Research Tomsk Polytechnic University, Russia, [5]Shubnikov Institute of Crystallography, FSRC "Crystallography and Photonics", RAS, Moscow, Russia, [6]Institute of Nanostructures and Biosystems, Saratov State University, Russia, [7]Institute for Photon Science and Synchrotron Radiation, Karlsruhe Institute of Technology, Germany, [8]Laboratory for Applications of Synchrotron Radiation, Karlsruhe Institute of Technology, Germany, [9]Centre for Organismal Studies, University of Heidelberg, Germany, [10]Dept. Sustainable Organic Chemistry and Technology, Ghent University, Belgium, [11]Laboratory of Pharmaceutical Technology, Ghent University, Belgium, [12]Dept. Analytical Chemistry, Ghent University, Belgium, Germany, [13]Centre for Nano- and Biophotonics, Ghent University, Belgium.

* E-mail: t.douglas@lancaster.ac.uk

Keywords: hydrogel, composite, micro-CT, gellan gum, bone cement

Abstract

Mineralized hydrogels are increasingly gaining attention as biomaterials for bone regeneration. The most common mineralization strategy has been addition of preformed inorganic particles during hydrogel formation. This maintains injectability. One common form of bone cement is formed by mixing particles of the highly reactive calcium phosphate alpha-tricalcium phosphate (α-TCP) with water to form hydroxyapatite (HA). The calcium ions released during this reaction can be exploited to crosslink anionic, calcium-binding polymers such as the polysaccharide gellan gum (GG) to induce hydrogel formation. In this study, three different amounts of α-TCP particles were added to GG polymer solution to generate novel, injectable hydrogel-inorganic composites. Distribution of the inorganic phase in the hydrogel was studied by high resolution microcomputer tomography (μCT). Gelation occurred within 30 minutes. α-TCP converted to HA. μCT revealed inhomogeneous distribution of the inorganic phase in the composites. These results demonstrate the potential of the composites as alternatives to traditional α-TCP bone cement and pave the way for incorporation of biologically active substances and *in vitro* and *in vivo* testing.

1. Introduction

Mineralized hydrogels are increasingly gaining attention as biomaterials for bone regeneration [1], and the most widespread mineralization strategy has been addition of preformed inorganic particles, most commonly calcium phosphate (CaP), to hydrogel precursors which become entrapped in the hydrogel network during gelation. This maintains hydrogel injectability, while promoting mechanical strength and growth and osteogenic differentiation of bone-forming cells [2,3].

Certain anionic polysaccharides, including gellan gum (GG), can be crosslinked with Ca^{2+} to form hydrogels [4]. Inorganic particles in GG solution may serve as delivery vehicles for slow release of Ca^{2+} to enable hydrogel formation [5-7], a process known as "internal gelation" [8]. For this, sufficient Ca^{2+} is a prerequisite. One highly reactive CaP type is alpha-tricalcium phosphate (α-TCP), which reacts with water to form crystals of calcium-deficient hydroxyapatite (CDHA), which can interlock mechanically to form bone cement [9].

α-TCP present in the studied materials hydrolyzes to a CDHA according to Equation 1:

$$3Ca_3(PO_4)_2 + H_2O \rightarrow Ca_9(HPO_4)(PO_4)_5(OH) \quad (1)$$

Hence, one would expect sufficient Ca^{2+} release from α-TCP to enable crosslinking of GG and subsequent internal gelation.

The creation of hydrogel-CaP composites combines the advantages of the CaP phase, i.e. mechanical reinforcement, bioactivity (the ability to form a direct chemical bond with surrounding bone) with the advantages of the hydrogel phase, i.e. straightforward addition of biologically active substances, such as antibacterial agents and growth factors to promote

bone regeneration, as well as bone-forming cells.

Addition of hydroxyapatite (HA) to hydrogels has been performed previously [3,10,11]. When preparing composites of GG hydrogels and a mineral phase, addition of α-TCP particles to GG solution has certain advantages over addition of pre-formed HA particles. Firstly, since the α-TCP particles release the crosslinker (Ca^{2+} ions), there is no need to add any further crosslinker to induce gelation. Addition of Ca^{2+} ions to GG solution at room temperature would result in instantaneous and inhomogeneous gelation, Secondly, the CDHA crystals formed by hydrolysis of α-TCP particles may be able to interlock mechanically to a greater degree than pre-formed HA particles. This would result in greater compressive strength and hardness, which is considered to be beneficial for osteogenic differentiation of bone-forming cells [12,13].

In this study, α-TCP was mixed with GG solution to create self-gelling, injectable hydrogel-inorganic composite biomaterials. The overall aim of the study was the physicochemical characterization of the composites to with a view to further *in vitro* and *in vivo* studies. Particular attention was paid to i) the rate of hydrogel formation, which was studied by rheometry; ii) the distribution of inorganic particles and their agglomerates, which was evaluated by high-resolution micro-computer tomography (μCT) and iii) the type of CaP present by X-ray diffraction (XRD), Fourier-transform infrared spectroscopy (FTIR), Raman spectroscopy and Scanning electron microscopy (SEM). Release of Ca and P from composites was also studied using Inductively-coupled optical emission spectroscopy (ICP-OES).

2. Materials and methods

All materials, including GG (G1910, "Low-Acyl", 200-300 kD), were acquired from Sigma-Aldrich, unless stated otherwise. α-TCP was produced as described previously [9]. α-TCP was

fully crystalline and sterilized thermally at 160°C for 3 hours. α-TCP particle size distributions were measured by laser diffraction (Mastersizer-S long bench, Malvern Instruments, Malvern, UK), using a wet dispersion technique. 100 mg α-TCP was dispersed in 10 mL 0.1% (w/v) aqueous polysorbate 80 solution and added to a MS1 Small Volume Dispersion unit (Malvern Instruments, Malvern, UK) to obtain 20% laser beam obscuration. The parameters were: 300RF lens, 2.4 mm active beam length, 1500 rpm stirrer speed, 6000 scans, polydisperse analysis model.

To produce composites, 1 mL pre-autoclaved (121°C for 15 min) aqueous 0.875% (w/v) GG solution was mixed with 300, 400 or 500 mg pre-sterilized α-TCP particles at room temperature in 2 mL Eppendorf tubes and shaken vigorously to yield 30, 40 or 50% (w/v) composites, hereafter referred to as GGa30, GGa40 and GGa50, respectively. The Eppendorf tubes served as moulds. This resulted in 1 mL roughly cylindrical samples of identical dimensions.

Rheometry was performed with an AR1000N Rheometer (TA Instruments) for 1800 s in triplicate as described previously (strain 0.1%, frequency 1 Hz, 37°C, plate-cone setup, cone diameter 4 cm) [7].

Release of elemental Ca and P was measured by incubating composites in Milli-Q water after gelation. Each composite was placed in 16 mL Milli-Q water. At each time point, 3 mL water was removed.for ICP-OES analysis. ICP-OES was performed using a Spectro Arcos Optical Emission Spectrometer (Spectro, Germany) as described previously [14]. Briefly, samples were mixed 1:1 (v:v) with 14 M analytical grade HNO_3 (ChemLab, Belgium). Samples were diluted with 0.3 M HNO_3 as necessary. Calibration was performed using standard solutions with Ca and P concentrations in the range 0-15 mg L^{-1}. Yttrium was used as an internal standard. For all measurements, n=3.

Injectability studies were performed based on the methods developed by Montufar et al [15-17]. 2

ml GG solution containing 30, 40 or 50% (w/v) α-TCP particles was added to a 5 ml syringe (Emerald™, BD, Belgium) with an orifice of internal diameter 2 mm. 0.2 ml was extruded every 1 minute by applying manual pressure. The measurement lasted 10 minutes.

After 7 d, μCT was performed with a laboratory X-ray tube (Detector Lab of Institute for Photon Science and Synchrotron Radiation, Karlsruhe Institute of Technology, Germany, Viscom X9160-D ED) set to 60 kV and 120 μA. For detection, a Dexela 1207 with a 150 μm CsI CMOS sensor (effective pixel size 74.8 μm) was used. To ensure focal spot limited spatial resolution, the source sample distance and source detector distance were adjusted to 3.5 cm and 70.0 cm, respectively, with total magnification of x20 resulting in effective pixel size of 3.7 μm and field of view 3.2 x 5.7 mm^2. For computed tomography, 1200 projection images were acquired over 360 ° degrees of sample rotation with the exposure time for each image of 4 s.

After 24 h, prior to XRD, FTIR, Raman and SEM, samples were dried at 60°C for 72 h and crushed into powders. XRD was performed with a Miniflex-600 diffractometer (Rigaku Corporation, Tokyo, Japan) using Cu-Kα radiation (40 kV, 15 mA, Ni-Kβ filter, 2θ range 5–60°, scan speed 7°/min). Crystalline phases were identified using integrated X-ray powder diffraction software (PDXL: Rigaku Diffraction Software) and ICDD PDF-2 datasets (Release 2014 RDB). Results were compared with known crystallographic data for hydroxyapatite (PDF#01-084-1998) [18]. FTIR was performed using a Perkin Elmer type Spectrum BX in ATR mode (attenuated total reflectance) over the wavenumber range 4000–550 cm^{-1} (32 scans, resolution of 4 cm^{-1}). as described previously [7].

SEM was performed with a MIRA II LMU (Tescan) at 20 kV in secondary electron mode. Prior to analysis, a drop of an aqueous suspension of the powder was air-dried on a silicon wafer at 22°C. Raman spectroscopy was performed with a WITec Alpha300R+ confocal Raman microscope equipped with a 785 nm excitation diode laser (Toptica) and

an UHTS 300 spectrometer with a -60 °C cooled CCD camera (ANDOR iDus 401 BR-DD) and an 100x/0.9 NA Nikon objective with lateral resolution 0.5 µm per pixel. 5 µL of a powder suspension in water (2.5 % (w/v)) was placed on a CaF plate and scanned (integration time 2 s, laser power 120 mW). Background subtraction was performed in R with in-house built scripts.

3. Results and Discussion

Laser diffraction measurements (Figure 1a) showed that sterilization had no effect on the size distribution of α-TCP particles. Representative rheometric measurements (Figure 1b) showed that hydrogel formation seemed to be approaching a maximum within 30 min, which would be acceptable for clinical applications. Storage modulus (G'), a measure of sample elasticity, decreased in the order GGa50 > GGa40 > GGa30. In addition, gelation speed decreased in the same order. Injectablility measurements revealed that all three composites could be extruded completely over 10 minutes, demonstrating injectability. ICP-OES measurements (Figure 1c) showed that release of elemental Ca and P from sample groups was similar for all sample groups at all time points. This suggests that a higher initial α-TCP content does not lead to higher Ca^{2+} release from the composites, which in turn would mean that quicker gelation and higher G' is not caused by higher Ca^{2+} release. It is also conceivable that higher initial α-TCP content leads to a greater contribution of particle-particle interactions to G'. Amounts of Ca and P released increased markedly from 3 h to 24 h to 48 h, suggesting that ion release continues over a longer time period, which may have consequences for hydrogel crosslinking.

µCT results (Figure 2a & 2b) revealed that CaP was distributed throughout the hydrogels. This distribution was not homogeneous. Regions of CaP were observed which were clearly

much larger than α-TCP particles. Inhomogeneity in the distribution of preformed ceramic particles has been reported previously [6,11]. Strategies to improve particle distribution include the use of dispersants such as sodium citrate [10]. In sample group GGa50, a larger number of small aggregates in the size range 10^3-10^4 μm^3 were observed (Figure 2c). This suggests superior dispersion of CaP within the composite, The reasons for this remain unclear. Greater homogeneity would be advantageous in order to promote more homogeneous regeneration of bone after implantation. A high concentration of CaP would be considered beneficial to aid bone regeneration. In this study, the maximum concentration of α-TCP particles added was 50% (w/v) (GGa50). Other authors have described the incorporation of up to 30% (w/v) HA in hydrogels of oligo(poly(ethylene glycol)fumarate) [3,10,11] or incorporation of up to 66% (w/v) HA in peptide amphiphile hydrogels functionalized with ligands[19]. 3% (w/w) PVA hydrogels have been enriched with 32% (w/w) α-TCP and subjected to hydrothermal treatment to convert α-TCP to rod-like HA crystals [20]. In this study, conversion of α-TCP to CDHA was achieved without hydrothermal treatment.

XRD, FTIR, SEM and Raman confirmed the transformation of α-TCP to CDHA in samples GGa30, GGa40 and GGa50. SEM (Figure 3a) revealed "star-like" deposits characteristic of CDHA. As secondary electron mode was used, lighter areas correspond to areas of increased charge and darker areas are due to areas of lower charge. Charging is not uncommon when studying CaP using SEM, especially as coating with a gold or carbon layer was not performed. XRD (Figure 3b) revealed peaks characteristic of CDHA. FTIR (Figure 3c) showed the presence of phosphate-specific bands characteristic of CDHA at 560 and 600 (υ^4 antisymmetrical bending), 962 (υ^1 symmetrical stretching) and 1022 cm^{-1} (υ^3 symmetrical bending) [21]. Raman (Figure 3d) showed bands characteristic for υ^1 symmetric stretching of phosphate groups at 961 cm^{-1} in aforementioned samples and 970 cm^{-1} in α-TCP. These are

typical for CDHA and α-TCP, respectively [22].

These results demonstrate the potential of the composites as alternatives to traditional α-TCP bone cement and pave the way for incorporation of biologically active substances and *in vitro* and *in vivo* testing. The physiochemical characterization data showed no difference in the type of mineral formed in GGa30, GGa40 and GGa50. Possibly, GGa50 could be most suitable composite for medical applications due to the superior mechanical strength and more homogeneous distribution of CaP.

This study has concentrated on physicochemical characterization of the composites. Further work is required to assess the biological performance of the composites both *in vitro* and *in vivo*. One potential advantage of combining α-TCP with the GG hydrogel phase is the incorporation of biologically active, water-soluble molecules in the hydrogel phase. This is a subject for future study. One possibility is inclusion of the enzyme alkaline phosphatase (ALP) and polydpoamine, which have induced and promoted mineralization of GG hydrogels in previous work [23]. Another possibility is inclusion of polyphenols, which can also promote GG hydrogel mineralization and impart antibacterial activity [24]. From a biological point of view, mineralization of GG with CDHA has resulted in superior adhesion and proliferation of osteoblast-like cells and superior osteoclast formation [23,25].

4. Conclusions

Addition of α-TCP to GG solution at 30, 40 and 50% (w/v) caused gelation within 30 min. α-TCP converted to CDHA, which was distributed inhomogeneously in the resulting composites. Release of Ca and P was similar for all composites. These novel composites may be an alternative to α-TCP bone cement. All three α-TCP concentrations induce hydrogel

formation and therefore all appear to be suitable.

5. Acknowledgement

Funding: This work was supported by FWO, Belgium [postdoctoral fellowships: T.E.L.D., B.V.P.], BOF UGent [A.G.S.] and the Era-Net Rus Plus project "Intelbiocomp" (contract ##14.587.21.0013 (a unique application number 2015-14-588-0002-5599)). V.W. and S.G. thank Dr. Elias Hamann (IPS, KIT) for assistance with µCT acquisition. X-ray measurements were performed using the equipment of the Shared Research Center of FSRC "Crystallography and Photonics" RAS.

6. Conflict of Interest, Ethical Approval, Original Publication and Author Contribution Statements

The authors have no conflict of interest. No benefit of any kind will be received either directly or indirectly by the authors. No ethical approval was required for this study. No part of this work has been previously published or submitted for publication elsewhere. The authors made the following contributions to the paper: Timothy E.L. Douglas conceived, designed, planned and coordinated the study, interpreted the data and wrote the majority of the manuscript. Josefien Schietse performed numerous preliminary experiments, produced the composites and performed rheometry (Figure 1b) and performed Ca and P release experiments (Figure 1c). Aneta Zima and Anna Słośarczyk produced and characterized the α-TCP. Svetlana Gorodzha Roman Shkarin, Venera Weinhardt, Tilo Baumbach, Maria A. Surmeneva and Roman A. Surmenev performed µCT measurements and interpreted the data (Figure 2a, 2b, 2c). Bogdan V. Parakhonskiy performed and interpreted XRD (Figure 3b)

Anna Ivanova performed and interpreted SEM (Figure 3a). Dmitry Khalenow performed and

interpreted Raman (Figure 3d). Chris Vervaet and Valérie Vanhoorne performed laser diffraction measurements (Figure 1a). Lieve Balcaen and Frank Vanhaecke performed ICP-OES analysis (Figure 1c). Christian V. Stevens performed FTIR (Figure 3c). Andre G. Skirtach co-coordinated the study and provided significant logistical help. All authors contributed to the interpretation of the results and the improvement of the discussion.

7. References

1. Gkioni K, Leeuwenburgh SC, Douglas TE, Mikos AG, Jansen JA. Mineralization of hydrogels for bone regeneration. Tissue Eng Part B Rev 2010;16(6):577-85.
2. Paxton JZ, Donnelly K, Keatch RP, Baar K. Engineering the bone-ligament interface using polyethylene glycol diacrylate incorporated with hydroxyapatite. Tissue Eng Part A 2009;15(6):1201-9.
3. Bongio M, van den Beucken JJ, Nejadnik MR, Leeuwenburgh SC, Kinard LA, Kasper FK, Mikos AG, Jansen JA. Biomimetic modification of synthetic hydrogels by incorporation of adhesive peptides and calcium phosphate nanoparticles: in vitro evaluation of cell behavior. Eur Cell Mater 2011;22:359-76.
4. Lee SK, Silva-Correia J, Caridade SG, Mano JF, Oliveira JM, Khang G, Reis RL. Evaluation of different formulations of gellan gum-based hydrogels for tissue engineering of intervertebral disc. J Tissue Eng Regen Med 2012;6:44-44.
5. Douglas TE, Piwowarczyk W, Pamula E, Liskova J, Schaubroeck D, Leeuwenburgh SC, Brackman G, Balcaen L, Detsch R, Declercq H and others. Injectable self-gelling composites for bone tissue engineering based on gellan gum hydrogel enriched with different bioglasses. Biomed Mater 2014;9(4):045014.
6. Gorodzha S, Douglas TE, Samal SK, Detsch R, Cholewa-Kowalska K, Braeckmans K, Boccaccini AR, Skirtach AG, Weinhardt V, Baumbach T and others. High-resolution synchrotron X-Ray analysis of bioglass-enriched hydrogels. J Biomed Mater Res A 2016.
7. Douglas TE, Lapa A, Reczynska K, Krok-Borkowicz M, Pietryga K, Samal SK, Declercq HA, Schaubroeck D, Boone M, Van der Voort P and others. Novel injectable, self-gelling hydrogel-microparticle composites for bone regeneration consisting of gellan gum and calcium and magnesium carbonate microparticles. Biomed Mater 2016;11(6):065011.
8. Chan LW, Lee HY, Heng PWS. Mechanisms of external and internal gelation and their impact on the functions of alginate as a coat and delivery system. Carbohydrate Polymers 2006;63(2):176-187.

9. Czechowska J, Zima A, Paszkiewicz Z, Lis J, Slosarczyk A. Physicochemical properties and biomimetic behaviour of alpha-TCP-chitosan based materials. Ceramics International 2014;40(4):5523-5532.
10. Leeuwenburgh SC, Ana ID, Jansen JA. Sodium citrate as an effective dispersant for the synthesis of inorganic-organic composites with a nanodispersed mineral phase. Acta Biomater 2010;6(3):836-44.
11. Leeuwenburgh SC, Jansen JA, Mikos AG. Functionalization of oligo(poly(ethylene glycol)fumarate) hydrogels with finely dispersed calcium phosphate nanocrystals for bone-substituting purposes. J Biomater Sci Polym Ed 2007;18(12):1547-64.
12. Evans ND, Minelli C, Gentleman E, LaPointe V, Patankar SN, Kallivretaki M, Chen X, Roberts CJ, Stevens MM. Substrate stiffness affects early differentiation events in embryonic stem cells. Eur Cell Mater 2009;18:1-13; discussion 13-4.
13. Rowlands AS, George PA, Cooper-White JJ. Directing osteogenic and myogenic differentiation of MSCs: interplay of stiffness and adhesive ligand presentation. Am J Physiol Cell Physiol 2008;295(4):C1037-44.
14. Gassling V, Douglas TE, Purcz N, Schaubroeck D, Balcaen L, Bliznuk V, Declercq HA, Vanhaecke F, Dubruel P. Magnesium-enhanced enzymatically mineralized platelet-rich fibrin for bone regeneration applications. Biomed Mater 2013;8(5):055001.
15. Montufar EB, Maazouz Y, Ginebra MP. Relevance of the setting reaction to the injectability of tricalcium phosphate pastes. Acta Biomater 2013;9(4):6188-98.
16. Montufar EB, Traykova T, Gil C, Harr I, Almirall A, Aguirre A, Engel E, Planell JA, Ginebra MP. Foamed surfactant solution as a template for self-setting injectable hydroxyapatite scaffolds for bone regeneration. Acta Biomater 2010;6(3):876-85.
17. Montufar EB, Traykova T, Schacht E, Ambrosio L, Santin M, Planell JA, Ginebra MP. Self-hardening calcium deficient hydroxyapatite/gelatine foams for bone regeneration. J Mater Sci Mater Med 2010;21(3):863-9.
18. Hughes JM, Cameron M, Crowley KD. Structural Variations in Natural F, Oh, and Cl Apatites. American Mineralogist 1989;74(7-8):870-876.
19. Anderson JM, Patterson JL, Vines JB, Javed A, Gilbert SR, Jun HW. Biphasic peptide amphiphile nanomatrix embedded with hydroxyapatite nanoparticles for stimulated osteoinductive response. ACS Nano 2011;5(12):9463-79.
20. Goto T, Kim IY, Kikuta K, Ohtsuki C. Hydrothermal synthesis of composites of well-crystallized hydroxyapatite and poly(vinyl alcohol) hydrogel. Materials Science & Engineering C-Materials for Biological Applications 2012;32(3):397-403.
21. Slosarczyk A, Paszkiewicz Z, Paluszkiewicz C. FTIR and XRD evaluation of carbonated hydroxyapatite powders synthesized by wet methods. Journal of Molecular Structure 2005;744:657-661.
22. Kolmas J, Kaflak A, Zima A, Slosarczyk A. Alpha-tricalcium phosphate synthesized by two

different routes: Structural and spectroscopic characterization. Ceramics International 2015;41(4):5727-5733.

23. Douglas T, Wlodarczyk M, Pamula E, Declercq H, de Mulder E, Bucko M, Balcaen L, Vanhaecke F, Cornelissen R, Dubruel P and others. Enzymatic mineralization of gellan gum hydrogel for bone tissue-engineering applications and its enhancement by polydopamine. J Tissue Eng Regen Med 2014;8:906–918.

24. Douglas TE, Dokupil A, Reczynska K, Brackman G, Krok-Borkowicz M, Keppler JK, Bozic M, Van Der Voort P, Pietryga K, Samal SK and others. Enrichment of enzymatically mineralized gellan gum hydrogels with phlorotannin-rich Ecklonia cava extract Seanol((R)) to endow antibacterial properties and promote mineralization. Biomed Mater 2016;11(4):045015.

25. Douglas TE, Krawczyk G, Pamula E, Declercq HA, Schaubroeck D, Bucko MM, Balcaen L, Van Der Voort P, Bliznuk V, van den Vreken NM and others. Generation of composites for bone tissue-engineering applications consisting of gellan gum hydrogels mineralized with calcium and magnesium phosphate phases by enzymatic means. J Tissue Eng Regen Med 2016;10(11):938-954.

8. Figure Captions

Figure 1: a) Size distribution of α-TCP particles before and after sterilization measured by laser diffraction analysis. b) Typical gelation curves for composites measured by rheometry. c) Release of elemental Ca and P from composites as a function of time. Mean values are displayed. Error bars show standard deviation.

Figure 2: µCT analysis of composites. a) 3D rendering of particles (red color) within GG (blue transparent color). b) Horizontal cross-sections through composites at four different heights (scale bar = 600 µm). c) Pie charts showing size distributions in four size categories of mineral agglomerates detected within composites. d) Bar charts showing number of mineral agglomerates in size categories ranging from 0 to 10^8 μm^3.

Figure 3: Physicochemical analysis of mineral within composites. a) SEM images. Scale bar = 2 µm (GGa30, GGa40) or 1 µm (GGa50). b) XRD diffractograms. The standard characteristic peaks of hydroxyapatite are marked. c) FTIR spectra. d) Raman spectra.

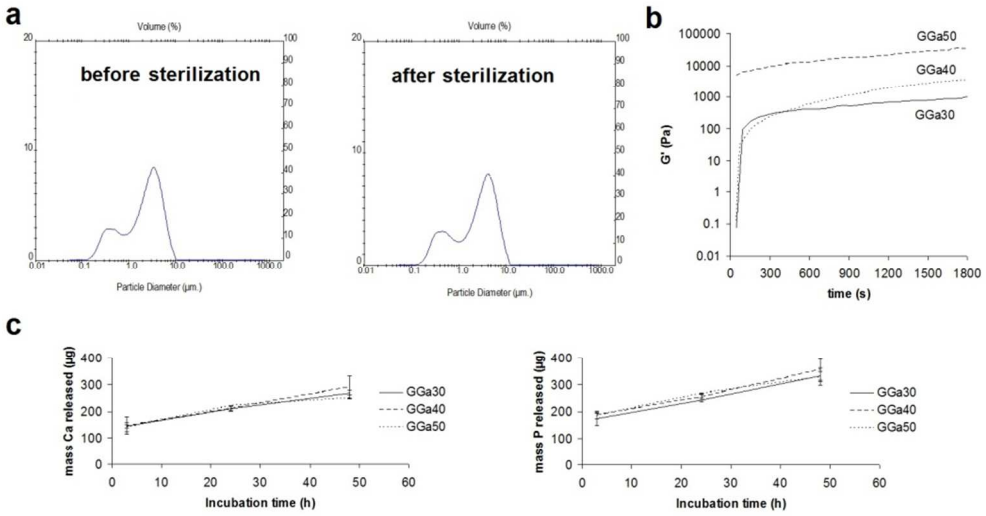

Figure 1: a) Size distribution of α-TCP particles before and after sterilization measured by laser diffraction analysis. b) Typical gelation curves for composites measured by rheometry. c) Release of elemental Ca and P from composites as a function of time. Mean values are displayed. Error bars show standard deviation.

90x48mm (300 x 300 DPI)

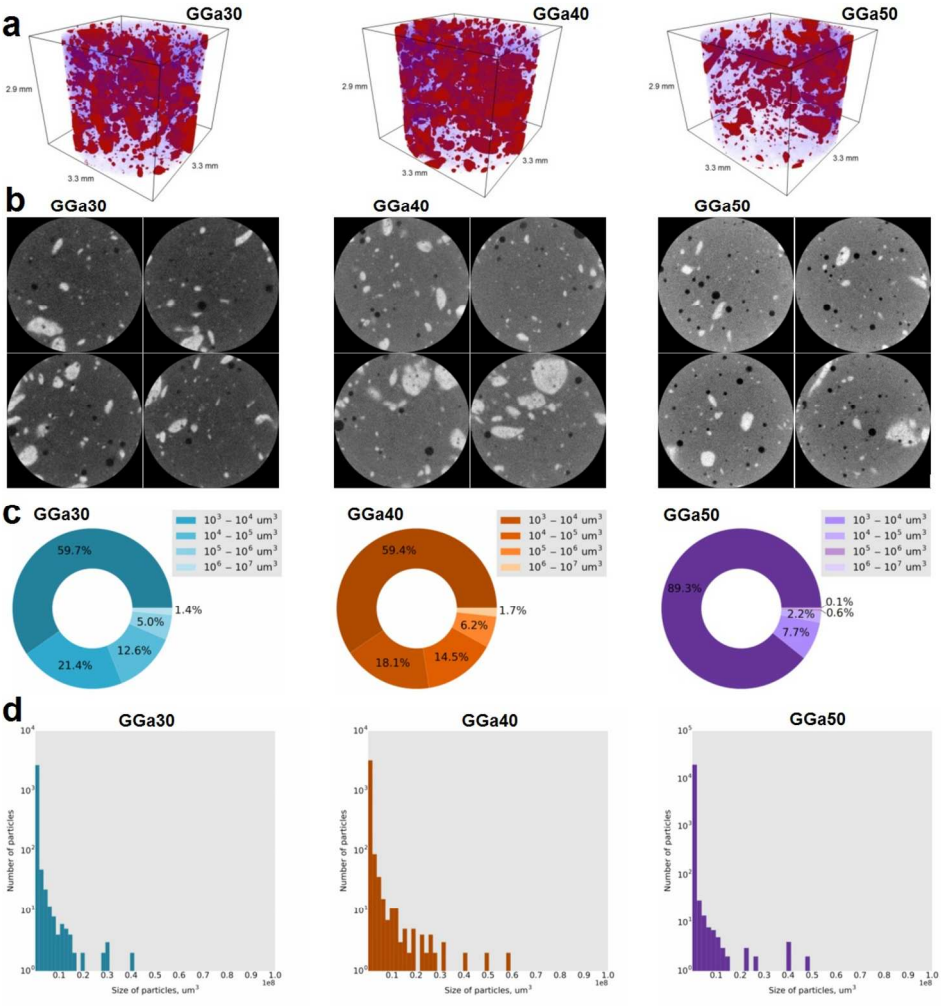

Figure 2: µCT analysis of composites. a) 3D rendering of particles (red color) within GG (blue transparent color). b) Horizontal cross-sections through composites at four different heights (scale bar = 600 µm). c) Pie charts showing size distributions in four size categories of mineral agglomerates detected within composites. d) Bar charts showing number of mineral agglomerates in size categories ranging from 0 to 108 µm3.

115x116mm (300 x 300 DPI)

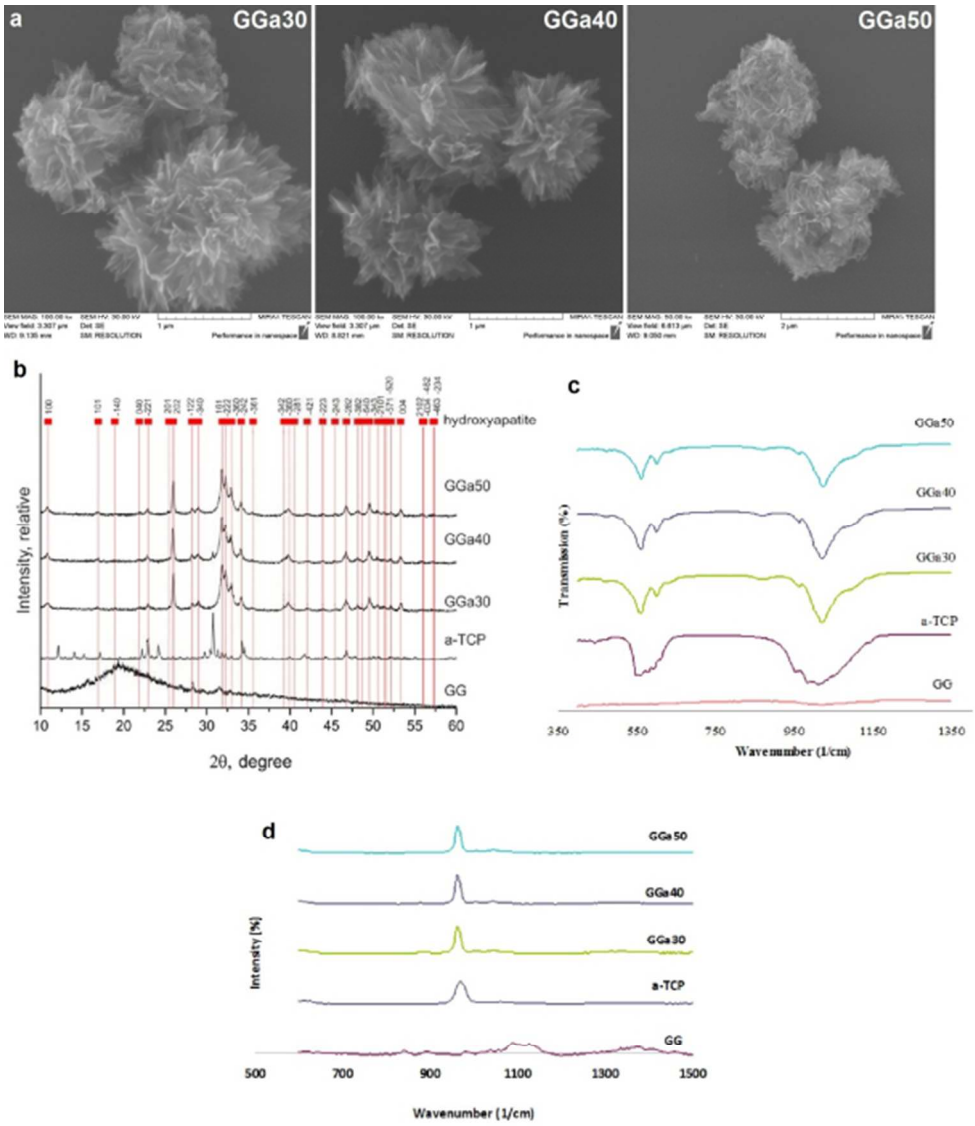

Figure 3: Physicochemical analysis of mineral within composites. a) SEM images. Scale bar = 2 μm (GGa30, GGa40) or 1 μm (GGa50). b) XRD diffractograms. The standard characteristic peaks of hydroxyapatite are marked. c) FTIR spectra. d) Raman spectra.

52x60mm (300 x 300 DPI)